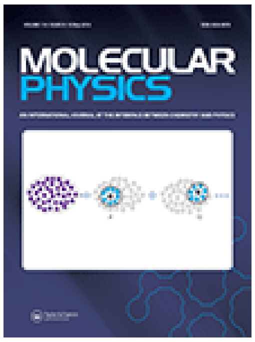

Taylor & Francis
Taylor & Francis Group

Molecular Physics

An International Journal at the Interface Between Chemistry and Physics

ISSN: (Print) (Online) Journal homepage: https://www.tandfonline.com/loi/tmph20

High-resolution anion photoelectron spectroscopy of cryogenically cooled 4-atom silicon carbides

Mark C. Babin , Martin DeWitt , Marissa L. Weichman , Jessalyn A. DeVine & Daniel M. Neumark

To cite this article: Mark C. Babin , Martin DeWitt , Marissa L. Weichman , Jessalyn A. DeVine & Daniel M. Neumark (2020): High-resolution anion photoelectron spectroscopy of cryogenically cooled 4-atom silicon carbides, Molecular Physics, DOI: 10.1080/00268976.2020.1817596

To link to this article: https://doi.org/10.1080/00268976.2020.1817596

MOLECULAR PHYSICS e1817596
https://doi.org/10.1080/00268976.2020.1817596

Taylor & Francis
Taylor & Francis Group

DAVID PARKER FESTSCHRIFT

High-resolution anion photoelectron spectroscopy of cryogenically cooled 4-atom silicon carbides

Mark C. Babin[a,b], Martin DeWitt[a,b], Marissa L. Weichman[a,b,†], Jessalyn A. DeVine[a,b,‡] and Daniel M. Neumark[a,b]

[a]Department of Chemistry, University of California, Berkeley, CA, USA; [b]Chemical Sciences Division, Lawrence Berkeley National Laboratory, Berkeley, CA, USA

ABSTRACT

High-resolution anion photoelectron spectra of cryogenically cooled Si_3C^-, $Si_2C_2^-$, and SiC_3^- obtained using slow photoelectron velocity-map imaging (cryo-SEVI) are presented, providing insight into the geometries, energetics, and vibronic structure of the anionic and the neutral clusters. These spectra yield accurate vibrational frequencies for the neutral clusters. They also yield refined adiabatic detachment energies (ADEs) for the ground states of Si_3C^- and $Si_2C_2^-$ of 1.5374(6) eV and 1.9019(4) eV, respectively, while the ADE of a low-lying isomer of SiC_3^- is found to be 1.9050(7) eV. The cryo-SEVI spectra show that the ground state of $Si_2C_2^-$ is a distorted trapezoid, and represent the first confirmation of the distorted trapezoid structure of Si_2C_2, the only low-lying isomer of this cluster with a permanent dipole moment. Additional transitions are observed from two low-lying anion isomers: a linear structure and a rhombus. The spectrum of SiC_3^-, in combination with electronic structure calculations, suggests that the true ground state of SiC_3 is a ring structure with a transannular C–C bond, addressing a longstanding controversy surrounding this cluster. All three spectra exhibit Franck-Condon forbidden transitions; these are attributed to Herzberg-Teller coupling in Si_3C and SiC_3 and autodetachment from an excited electronic state of $Si_2C_2^-$.

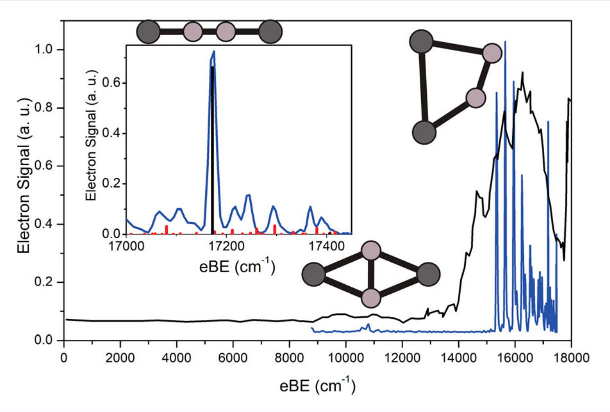

ARTICLE HISTORY
Received 18 August 2020
Accepted 25 August 2020

KEYWORDS
Photoelectron spectroscopy; ion spectroscopy; clusters

Introduction

Small silicon carbides (Si_mC_n) are of considerable fundamental and applied interest as potential building blocks for the synthesis of novel nanoscale materials [1], for their role in the low-pressure vapour deposition of solid silicon carbide [2], and based on their detection in the circumstellar envelope of carbon-rich stars such as IRC+10216 [3–8]. Since these clusters are intermediate between the pure carbon (C_n) and silicon (Si_n) clusters, whose structural trends are well documented [9–17], they provide an excellent system to explore the nature of the organosilicon bond, potentially

---

CONTACT Daniel M. Neumark dneumark@berkeley.edu Department of Chemistry, University of California, Berkeley, CA 94720, USA; Chemical Sciences Division, Lawrence Berkeley National Laboratory, Berkeley, CA 94720, USA

[†] Current address: Department of Chemistry, Princeton University, Princeton, New Jersey 08544, USA

[‡] Current address: Department of Dynamics at Surfaces, Max-Planck Institute for Biophysical Chemistry, Am Faßberg 11, 37077 Göttingen, Germany

Supplemental data for this article can be accessed here. https://doi.org/10.1080/00268976.2020.1817596

aiding in the engineering of nanostructured silicon carbides and assignment of astronomical data. These considerations have motivated myriad experimental and theoretical studies utilising matrix isolation infrared spectroscopy [18,19], Fourier transform microwave spectroscopy [6,7,20–22], resonant two-color two-photon ionisation (R2C2PI) [23–25], infrared-ultraviolet two-color ionisation (IR-UV2CI) [26], anion photoelectron spectroscopy (PES) [27,28], and electronic structure calculations [23,29–46], all aimed at characterising the electronic and vibrational structure of small silicon carbides. Despite this extensive body of work, the Si_nC_m ($n + m = 4$) clusters still pose a significant challenge to both theory and experiment. In this work, we address longstanding questions surrounding the structures of Si_3C, Si_2C_2, and SiC_3 using high resolution photoelectron spectroscopy of cryogenically cooled anions and high-level *ab initio* calculations.

Proposed structures for the ground states of the 4-atom silicon carbide clusters ($Si_3C^{0/-}$, $Si_2C_2^{0/-}$, and $SiC_3^{0/-}$) are shown in Figure 1. Si_3C is perhaps the best characterised of the three clusters. First detected in 1992 by Graham and co-workers [18] using FTIR of vaporised silicon carbides trapped in Ar matrices, five of six vibrational modes were reported and its structure was unambiguously determined as a 4-membered ring with a transannular Si–C bond (structure 1a). Since then, this structure of Si_3C has been confirmed by a number of gas-phase experiments [23–27] and calculated to be the ground state of this species [23,35,36,41], while anion photoelectron spectroscopy of Si_3C^- has confirmed the ground state of the anion as structure 1a [27].

It has been more challenging to characterise the ground states of the two other four-atom clusters. The ground state of neutral Si_2C_2 has been calculated to be a rhombic structure (2b) [30–33,36,38,39,45], lying less than 40 kJ/mol below both a linear isomer and a distorted trapezoid (2c,d, respectively), while the energetic ordering of structures 2c and 2d is method-dependent. This uncertainty was complicated when Graham and co-workers [19] observed vibrational bending modes tentatively assigned to all three isomers via Ar matrix FTIR spectroscopy. Since then, a recent R2C2PI study from Steglich and Maier [25] observed only contributions from the linear isomer (2c) in their jet-cooled expansion, though their probe energies are below the calculated IE of structure 2b, and the authors make no mention of 2d. Anion photoelectron spectroscopy by the Kaya group [27] showed both sharp and broad features, attributed to photodetachment from two anion isomers, but definitive assignments were hampered by the absence of resolved vibrational structure. Theoretical efforts to explain this spectrum have found either structure 2c or 2d to be the ground state for the $Si_2C_2^-$ anion [36,38,45].

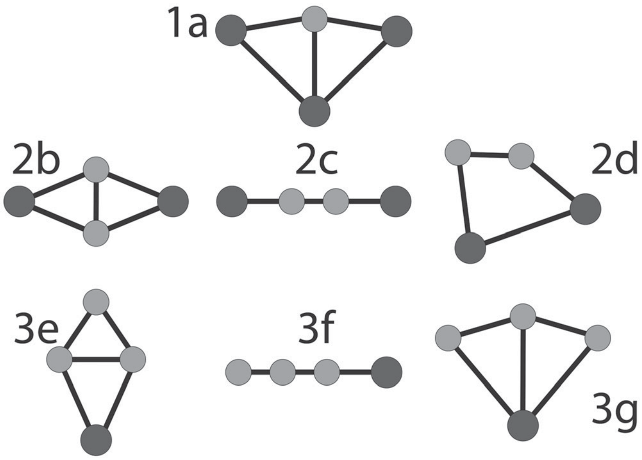

Figure 1. Structures of low-lying isomers of Si C (1a), Si C (2b-d), and SiC (3e-g).

SiC_3 is perhaps the most contentious of the three. The ground state was first calculated to be a four-membered ring with a transannular C–C bond (3e), with a low-lying linear triplet state and a second rhomboidal Si–C transannular bonding structure (3f and 3 g, respectively) within 20 kJ/mol [34,37]. Structure 3e was discovered shortly thereafter not only in the laboratory [7,21], but also in the interstellar medium [6]. Subsequently, McCarthy *et al.* detected both structure 3 g and 3f in a supersonic molecular beam via FT-microwave spectroscopy [20,22]. Following this, numerous experimental and theoretical studies were performed to ascertain the true ground state of SiC_3, with theorists determining the three structures lie withing a few kJ/mol of one another, though the ordering is method-dependent [29,36,39,40,42–46]. Anion photoelectron spectra revealed both sharp structure at high binding energies, assigned to the linear structure 3f by the Kaya group and confirmed by the Lineberger group, and two broad, weak features at lower binding energies attributed to the presence of one or more ring structures [27,28]. These studies were able to confirm the lowest-energy structure of SiC_3^- as the 3f linear species, in agreement with theory that suggests this structure is at least 40 kJ/mol more stable than either of the two ring isomers (3e,g) [36,37,45].

The present study uses slow photoelectron velocity-map imaging of cryogenically cooled anions (cryo-SEVI) [47] to obtain photoelectron spectra with highly resolved vibrational structure of Si_3C^-, $Si_2C_2^-$, and SiC_3^-. With the aid of Franck-Condon (FC) simulations, all bands are unambiguously assigned to specific structural isomers of the three clusters. Investigation into Si_3C^- allows for determination of the frequency for the previously unreported ν_4 vibrational mode, with features having odd quanta along this mode appearing via Herzberg-Teller coupling. Our spectrum of $Si_2C_2^-$ reveals detachment from three anionic isomers, and establishes the distorted trapezoid 2d as the ground state of $Si_2C_2^-$. Significant FC-activity from photodetachment of structure 2d allows for characterisation of the vibrational frequencies of the corresponding neutral species, including FC-forbidden transitions along the ν_6 normal mode that gains intensity through vibrational autodetachment. The cryo-SEVI spectrum of SiC_3^- provides the first information on the vibrational structure 3e of SiC_3, revealing non-FC activity along the ν_4 normal coordinate. Collectively, these spectra provide improved ADEs for structures 1a, 2b,c,d, and 3e, allowing for the determination of upper bounds for the energetic splitting of the neutral silicon carbide clusters. Coupling these experimental ADEs with *ab initio* calculations and experimental considerations suggests that the true ground sate of SiC_3 is a ring containing a transannular C–C bond (3e).

Experimental methods

The cryo-SEVI method has been described in detail previously [47–50]. In this work, silicon carbide cluster anions are generated with a laser ablation source using a frequency-doubled Nd:YAG laser focused onto a rotation and translating silicon carbide disk. The resulting plasma is entrained within a pulse of He carrier gas from an Even-Lavie solenoid valve [51] before passing through a skimmer. The ions then pass through a radiofrequency (RF) hexapole ion guide and a RF quadrupole mass filter and are directed into a linear RF octupole ion trap held at 5 K and filled with a buffer gas mixture of 20:80 H_2:He. Collisions with the cold buffer gas result in effective vibrational, rotational, and electronic cooling of the ions, leading to internal temperatures near 10 K [47,52,53].

After ∼40 ms, the ions are extracted from the trap into an orthogonal Wiley-McLaren time-of-flight mass spectrometer [54] and focused into the interaction region of a seven-plate velocity-map imaging (VMI) electrostatic lens assembly [55,56]. In the VMI spectrometer, ions are photodetached by the output of a dye laser pumped by the second harmonic of a Nd:YAG laser operating at 20 Hz.

The resulting photoelectrons are projected onto a 2D detector comprising two chevron-stacked microchannel plates coupled to a phosphor screen, which is photographed by a CCD camera after each laser shot [57]. Each image is analyzed for individual electron events for which the centroids are calculated and binned in a 1024 × 1024 grid [58]. The three-dimensional electron velocity distribution is reconstructed from the accumulated images using the Maximum Entropy Velocity Legendre Reconstruction (MEVELER) algorithm [59]. The radial position of features in the reconstructed image is related to electron kinetic energy (eKE) by acquiring VMI images for detachment from atomic O^- at several photon energies [60].

The VMI spectrometer has an approximately constant resolving power, ΔeKE/eKE [55], yielding the best eKE resolution for slow electrons. As such, a SEVI spectrum is acquired by first taking an overview spectrum at a relatively high photon energy before tuning the detachment laser to energies slightly above features of interest. This procedure results in a series of high-resolution spectra over narrow energy windows that are concatenated and scaled to match intensities in the overview spectrum, which is less sensitive to variation of the photodetachment cross section with photon energy. Spectra are plotted as a function of electron binding energy (eBE), given by $\mathrm{eBE} = h\nu - \mathrm{eKE}$.

In addition to the eKE distributions, VMI allows for the determination of photoelectron angular distributions (PADs) associated with each detachment transition, given by [61]

$$\frac{d\sigma}{d\Omega} = \frac{\sigma_{\text{tot}}}{4\pi}[1 + \beta P_2(\cos\theta)], \tag{1}$$

where σ_{tot} is the total detachment cross section, $P_2(x)$ is the second-order Legendre polynomial, θ is the angle of the outgoing photoelectron velocity vector with respect to the laser polarisation axis, and β is the anisotropy parameter. The anisotropy parameter, which ranges from -1 (perpendicular detachment) to $+2$ (parallel detachment), reflects the angular momentum of the detached electron and is thus tied to the electronic character of each photodetachment transition [62].

Computational methods

Electronic structure calculations for all isomers of $Si_3C^{0/-}$ and $Si_2C_2{}^{0/-}$ were carried out at the CCSD/aug-cc-pVDZ level of theory, while those for $SiC_3{}^{0/-}$ were carried out at the CCSD/aug-cc-pVTZ level [63–65]. Based on the calculated energetics of these species in previous work [23,29–32,34,36,39,40, 43,45,46], the calculations were restricted to the singlet manifold for all ring structures (1a, 2b, 2d, 3e, and 3g), while both the singlet and triplet structures for the linear isomers (2c, 3f) were considered. All calculations were performed using Gaussian 16 (revision A.03) [66]. Calculated adiabatic detachment energies (ADEs) are zero-point corrected. Calculated geometries are presented in

Tables S1–18 while the energetics of the anion and neutral isomers are listed in Tables S19 and S20.

The equilibrium geometries and normal modes were used to calculate the Franck-Condon (FC) profiles for the relevant photodetachment transitions in Si_3C^-, $Si_2C_2^-$, and SiC_3^- with the ezSpectrum v3.0 software package [67]. All modes were treated in the harmonic approximation and FC integrals were calculated using full Duschinsky mixing of all normal modes [68]. To better match experiment, FC simulations use experimentally determined frequencies when available. The calculated and experimental values used in these simulations are presented in Tables S21–23 of the SI, while cryo-SEVI spectra with FC simulations using the calculated frequencies are presented in Figures S1–7 of the SI. In the case of $Si_2C_2^-$ and SiC_3^-, discrepancies between the simulated FC profiles and experiment were observed when the calculated structures were used. These were addressed by making small additional displacements to either the anion or neutral normal coordinates. Adjustments were made to the Si_2C_2 structure on the basis of better agreement between the calculated and experimental ADE for the distorted neutral species; this point is discussed in more detail in the SI. For SiC_3^-, adjustments were made to the anion as microwave spectra have provided accurate experimental bond-lengths for the neutral species. Full details of these adjustments are presented in Sections S1 and S2 of the SI.

Excited state energies for the Si_3C, $Si_2C_2{}^{0/-}$, and SiC_3 clusters were calculated using the equation of motion coupled cluster (EOM-CCSD) framework [69–74] with the same basis set as used for geometry optimizations within Gaussian 16. Calculations were performed using the optimised ground state geometries unless otherwise stated. Term energies and state symmetries of the first four excited states are presented in Table S24 of the SI.

Results

The cryo-SEVI spectra of Si_3C^-, $Si_2C_2^-$, and SiC_3^-, are presented in Figures 2–4 respectively. In these panels, a low-resolution overview spectrum (blue) is displayed atop high-resolution composite spectra (black) taken at several photon energies as well as simulated Franck-Condon profiles (red sticks) using adjusted geometries as described above [63–65]. Peak assignments, electron binding energies (eBEs), and shifts from peak A are given in Tables 1–3 for Si_3C, Si_2C_2, and SiC_3, respectively. A complete listing of experimental parameters determined here with a comparison to literature values is included in Table 4. Computationally determined geometries, theoretical relative energetics of differing isomers, and spectra with FC simulations using calculated frequencies are presented in Figures S1–7 and Tables S1–S24 of the SI.

The cryo-SEVI spectra of Si_3C, Si_2C_2, and SiC_3 represent significant improvements over previous anion photoelectron spectroscopy studies [27,28]. The improved resolution afforded by the cryo-SEVI method reveals a strong vibrational origin (peak A) followed by a progression of transitions to vibrationally excited states of the neutral clusters. Vibrational assignments are facilitated by comparison between FC simulations and the experimental spectra.

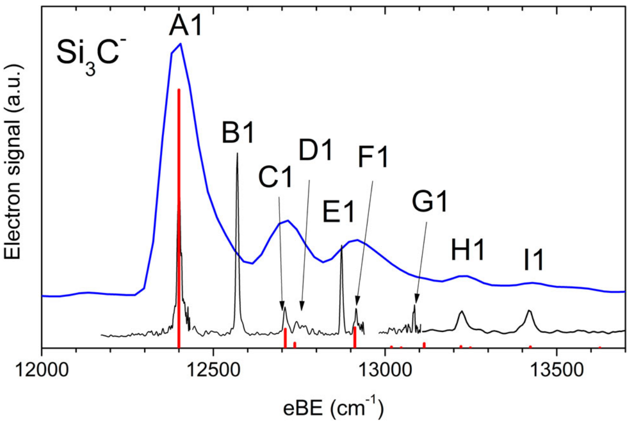

Figure 2. Cryo-SEVI spectra of Si_3C^-. A low-resolution spectrum (blue) sits above both high resolution scans (black, variable photon energies) and a simulated photoelectron stick spectrum for structure 1a (red).

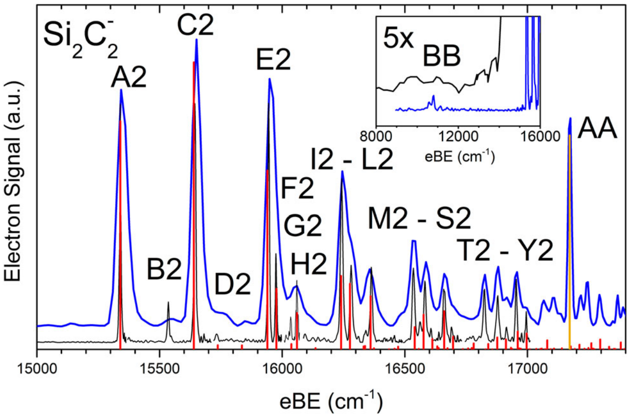

Figure 3. Cryo-SEVI spectra of $Si_2C_2^-$. A low-resolution spectrum (blue) sits above both high resolution scans (black, variable photon energies) and a simulated photoelectron stick spectrum for structures 2d (red) and 2c (gold). Insert: magnification of low eBE region displaying weak cryo-SEVI signal (blue) below PES spectrum of Kaya *et al.* (black) [27].

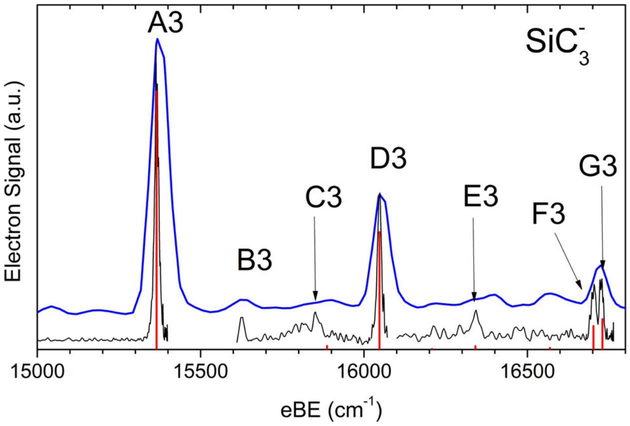

Figure 4. Cryo-SEVI spectra of SiC_3^-. A low-resolution spectrum (blue) sits above both high resolution scans (black, variable photon energies) and a simulated photoelectron stick spectrum (red).

Table 1. Peak positions, shifts from peak A1, and assignments for the detachment transitions in the cryo-SEVI spectrum of Si_3C presented in Figure 2.

Peak	eBE (cm^{-1})	Shift (cm^{-1})	Assignment
A1	12400(9)	0	0^0_0
B1	12570(7)	170	4^1_0
C1	12710(10)	309	3^1_0
D1	12743(13)	343	4^2_0
E1	12873(7)	473	$3^1_0 4^1_0$
F1	12914(15)	514	2^1_0
G1	13084(6)	684	6^2_0
H1	13224(21)	824	$2^1_0 3^1_0$
I1	13420(25)	1019	2^2_0

Note: Uncertainties in peak positions correspond to one standard deviation obtained from a Gaussian fit to the corresponding feature in the high-resolution scan.

Table 2. Peak positions, shifts from peak A2, and assignments for the detachment transitions in the cryo-SEVI spectrum of Si_2C_2 presented in Figure 3.

Peak	eBE (cm^{-1})	Shift (cm^{-1})	Assignment
A2	15340(6)	0	0^0_0
B2	15536(7)	196	6^1_0
C2	15645(7)	305	5^1_0
D2	15733(9)	393	6^2_0
E2	15945(7)	605	5^2_0
F2	15975(7)	636	3^1_0
G2	16035(4)	695	$5^1_0 6^2_0$
H2	16060(8)	720	2^1_0
I2	16242(10)	903	5^3_0
J2	16281(9)	941	$3^1_0 5^1_0$
K2	16343(15)	1003	4^2_0
L2	16363(8)	1024	$2^1_0 5^1_0$
M2	16535(10)	1195	5^4_0
N2	16563(7)	1223	$2^1_0 4^2_0$
O2	16582(8)	1242	$3^1_0 5^2_0$
P2	16606(6)	1267	3^2_0
Q2	16639(4)	1299	$5^3_0 6^2_0$
R2	16661(9)	1321	$2^1_0 5^2_0$
S2	16691(6)	1351	$2^1_0 3^1_0$
T2	16824(9)	1484	5^5_0
U2	16878(10)	1538	$3^1_0 5^3_0$
V2	16914(7)	1574	$3^2_0 5^1_0$
W2	16954(7)	1614	$2^1_0 5^3_0$
X2	16976(4)	1636	$3^1_0 5^1_0 6^2_0$
Y2	16995(5)	1655	$2^1_0 3^1_0 5^1_0$
AA	17171(13)	1832	0^0_0 (2c, see text)

Note: Uncertainties in peak positions correspond to one standard deviation obtained from a Gaussian fit to the corresponding feature in the high-resolution scan. Assignments are for isomer 2d unless stated otherwise.

Table 3. Peak positions, shifts from peak A3, and assignments for the detachment transitions in the cryo-SEVI spectrum of SiC_3 presented in Figure 4.

Peak	eBE (cm^{-1})	Shift (cm^{-1})	Assignment
A3	15365(12)	0	0^0_0
B3	15626(15)	261	4^1_0
C3	15850(9)	485	4^2_0
D3	16047(11)	682	3^1_0
E3	16341(21)	976	2^1_0
F3	16702(15)	1337	1^1_0
G3	16726(12)	1361	3^2_0

Note: Uncertainties in peak positions correspond to one standard deviation obtained from a Gaussian fit to the corresponding feature in the high-resolution scan.

Discussion

Spectral assignments

Si_3C

The cryo-SEVI spectrum of Si_3C^- is presented in Figure 2 along with FC simulations for structure 1a, selected as this structure is known to be the ground state of $Si_3C^{0/-}$ [18,23–25,35,36]. In this spectrum, features C1, D1, F1, G1, H1, and I1 are reproduced in the FC simulations, allowing for their assignment as the 3^1_0, 4^2_0, 2^1_0, 6^2_0, $2^1_0 3^1_0$, and 2^2_0 transitions. From these peak locations the frequencies of the ν_2, ν_3, and ν_6 normal modes of Si_3C may be inferred, as reported in Table 4; these values are in good agreement with those determined by Graham *et al.* [18] Though features B1 and E1 are notably absent from our FC simulations, their shifts from peak A1 match well with the FC-forbidden 4^1_0 and $3^1_0 4^1_0$ transitions, the appearance of which is discussed below. As feature B1 reports on the 4^1_0 transition, its position allows for the determination of the out-of-plane ν_4 normal mode in this species for the first time. Our experimental value of $\nu_4 = 170(6)$ cm^{-1} is in good agreement with our calculated value of 168 cm^{-1} as well as those reported in previous theoretical work [23,35].

As both features B1 and E1 report on transitions involving odd quanta along the non-totally symmetric ν_4

Table 4. Experimental parameters for structures 1a, 2d, and 3e of SiC_3, Si_2C_2, and SiC_3, respectively, extracted from the cryo-SEVI spectrum of the corresponding anion, comparison to theoretical values obtained in the current work (CCSD/aug-cc-pVXZ, X = T for SiC_3, X = D for Si_3C, Si_2C_2), and available literature values.

	Si_3C			Si_2C_2			SiC_3		
Parameter	Calc	SEVI	Lit	Calc	SEVI	Lit	Calc	SEVI	Lit
ADE (eV)	1.349	1.5374(6)	1.54(8)[a]	1.720	1.9019(4)	1.93(8)[a]	1.807	1.9050(7)	1.93(10)[a]
ν_1 (a_1), (a')	635		658.2[b]	1571			1429	1337(10)	
ν_2 (a_1), (a')	501	514(9)	511.8[b]	698	720(5)		982	976(12)	
ν_3 (a_1), (a')	299	309(7)	309.5[b]	616	636(4)	632[c]	675	682(8)	
ν_4 (b_1), (a')	169	170(6)		482	501(11)		261	261(10)	
ν_5 (b_2), (a')	1081		1101.4[b]	296	305(5)		1069		
ν_6 (b_2), (a')	343	342(8)	357.6[b]	193	196(5)		401		

Note: Reported ADEs are for the corresponding anions. Vibrational mode symmetries for Si_3C and SiC_3 are listed first, then those for Si_2C_2. All values are in cm^{-1} unless otherwise stated.

[a] Ref [27]; [b] Ref [18]; [c] Ref [19].

mode, they are formally FC-forbidden, and their appearance is ascribed to Herzberg-Teller (HT) coupling to an excited neutral state. The signatures of HT coupling in anion photoelectron spectroscopy are well established, and come about due to borrowed electronic character from an excited state [75–84]. Transitions that are allowed only through HT coupling often have different photoelectron angular distributions than FC-allowed peaks. Moreover, in cryo-SEVI spectra, HT coupling leads to different relative intensities compared to FC allowed transitions as the photodetachment energy is varied, an effect that can be particularly pronounced when the electron kinetic energies are low. Comparison of the overview and high-resolution composite transitions in Figure 2 show that peaks B1 and E1 are enhanced at low eKE relative to FC-allowed transitions (see also Figure S8), an effect also seen in the cryo-SEVI spectrum of NO_3^- [84].

Si_2C_2

The cryo-SEVI spectrum of Si_2C_2 reveals substantially more vibrational structure than Si_3C. We find poor agreement between FC simulations for structures 2b and 2c of Si_2C_2 (Figures S1, 2 in the SI). FC simulations for structure 2d using the calculated geometries fare considerably better but overestimate the activity along the ν_2 and ν_3 normal coordinates. This is corrected for by adjusting the optimised geometry along the neutral ν_3 and ν_2 normal coordinates, bringing the observed structure closer to a C_{2v} trapezoid (see Section S1 and Figures S3, 4 of the SI). The resulting FC simulations involving the adjusted-Si_2C_2 structure, presented in Figure 3, are in excellent agreement with the experimental results. These simulations facilitate the assignment of nearly every transition observed in the cryo-SEVI spectrum, including the 2_0^1, 3_0^1, 5_0^1, 4_0^2, and 6_0^2 transitions (features H2, F2, C2, K2, and D2, respectively), as shown in Table 2. These assignments allow for the determination of the vibrational frequencies of the ν_2, ν_4, ν_5, and ν_6 modes of Si_2C_2 for the first time, while our experimentally determined value of 636(4) cm^{-1} for ν_3 in good agreement with the tentative assignment provided by Graham [19].

Peak B2 is not reproduced by our FC simulations, but the position of this features matches well with the expected location of the FC-forbidden 6_0^1 transition. Unlike peaks B1 and E1 in the spectrum of Si_3C^-, feature B2 in $Si_2C_2^-$ only appears in one of 12 scans taken over a range of photon energies (Figure S9), a clear indication of autodetachment from an excited anionic state [85–89]. Vibrational autodetachment is a non-Born-Oppenheimer process wherein vibrational and rotational degrees of freedom couple the autodetaching anionic excited state to the (neural + free electron) continuum, permitting the observation of otherwise inaccessible neutral states [90,91]. In the present study, peak B2 is only observed when detached with a photon energy of 1.94930 eV (15,722 cm^{-1}), residing very near our calculated term energy of 1.9560 eV at the EOM-CCSD/aug-cc-pVDZ level for the $\tilde{C}$ state of structure 2d of $Si_2C_2^-$ and only 11 cm^{-1} below the calculated position of the FC-allowed 6_0^2 transition. As vibrational autodetachment preferentially occurs by loss of one vibrational quantum ($\Delta\nu = -1$) in a coupling mode whose normal coordinate changes the character of the anion orbital from which the electron is autodetached [90], these results strongly suggest that the observed 6_0^1 transition in Si_2C_2 is facilitated by vibrational autodetachment from the $2\nu_6$ level of the $\tilde{C}$ state in $Si_2C_2^-$.

Our cryo-SEVI spectra also show evidence for contributions from multiple isomers; as shown in Figure 3, we see signal at ~ 10,500 cm^{-1} (peak BB) and 17,172 cm^{-1} (peak AA) that has previously been attributed to other structures of Si_2C_2 by Kaya *et al.* [27] Feature BB is exceptionally weak and was collected at high eKE, producing a spectrum with low resolution that is assigned as structure 2b on the basis of previous assignments. At high eBE we observe an isolated sharp feature, peak AA, that clearly lies beyond the FC simulation for structure 2d. This peak is assigned to linear Si_2C_2 (structure 2c); it is reproduced by FC simulations for detachment from the linear anion that exhibit a strong vibrational origin without any other features of discernible intensity. Such a result agrees with previous findings on linear carbon and silicon carbide clusters that find photoelectron spectra dominated by a sharp vibrational origin and lacking an extended vibrational progression [27,28,92–95].

SiC_3

The cryo-SEVI spectra of SiC_3 represents an investigation into the lowest-eBE region of previously reported PES spectra, ascribed to detachment from a low-lying ring structure of SiC_3^- in those studies [27,28,37]. The current work displays the first vibrationally-resolved spectrum in this region, allowing for the assignment of structure 3e as the origin of this band based on agreement between simulated FC profiles for this structure (as reported in Figure 4) and poor agreement for structure 3 g. As detachment from linear SiC_3^- has been observed by Lineberger with a band origin at eBE higher than those explored in this work [75], structure 3f was excluded from consideration.

FC profiles based on the optimised 3e geometry underreport activity in ν_3 and require additional displacement along the corresponding normal coordinate to adequately reproduce features C3, D3, E3, F3 and G3 in the experimental spectrum (see Section S2 and Figures S6, 7). The FC-simulations using this adjusted anion geometry are presented in Figure 4 and allow for the assignment of these peaks to the 4_0^2, 3_0^1, 2_0^1, 1_0^1, and 3_0^2 transitions, respectively. From these assignments, we are able to extract experimental frequencies for the ν_1, ν_2, ν_3, and ν_4 normal modes for the first time, as shown in Table 4 below. Feature B3 is once again not reproduced by our FC simulations. As the position of this feature aligns with the FC-forbidden 4_0^1 transition, a detachment cross section that diminishes more rapidly than the FC-allowed features as its photodetachment threshold is approached (see Figure S10 in SI), and a photoelectron angular distribution that differs from peak A3 (Figure S11 in SI), we assign this feature to the 4_0^1 transition that gains intensity through HT-coupling.

Isomers and energetics

Adiabatic detachment energies (ADE) are experimentally determined for each observed anion isomer by the position of the vibrational origin of the corresponding band in the cryo-SEVI spectrum. For Si_3C^- and SiC_3^-, the lowest energy transitions (peak A) yield ADEs of 1.5374(6) eV and 1.9050(7) eV for structures 1a and 3e, respectively. In the case of $Si_2C_2^-$, structures 2b, 2c, and 2d are found to have ADEs of 1.30 eV, 2.1291(8) eV, and 1.9019(4) eV, respectively. These values represent an improvement by two orders of magnitude from those previously reported for structures 1a, 2c, and 2d [27], and represent the first reported value for structures 2b and 3e.

An ADE is equal to the electron affinity of a particular Si_mC_n cluster only when the vibrational origin transition is between the anion and neutral ground state structures. Moreover, the photoelectron spectra of $Si_2C_2^-$ and SiC_3^- presented here and elsewhere exhibit multiple bands, but these do not involve photodetachment from common isomers. For this reason, these spectra alone do not provide enough information to constrain the relative energy ordering of isomers in either the neutral or anionic manifolds. Nonetheless, by comparing experiment and theory, one can obtain information on the anion and neutral energy orderings and place limits on the energy splittings between the various neutral and anion isomers. These

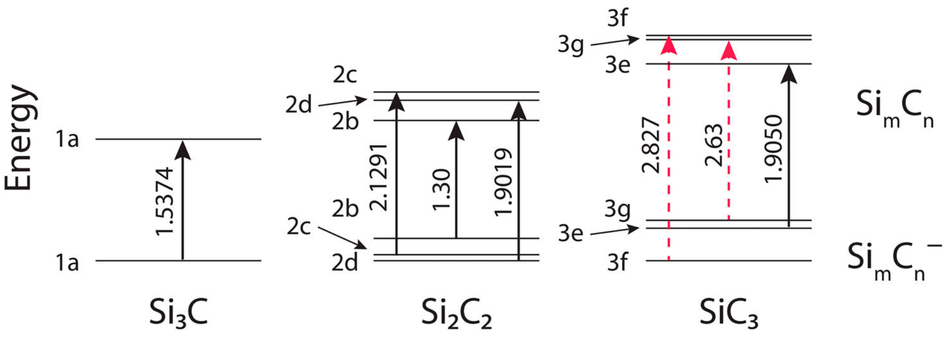

Figure 5. Energy level diagram of the various isomers and charge states of Si_3C, Si_2C_2, and Si_2C_2. Depicted level splittings for the anion and neutral manifolds are from our CCSD calculations, while the reported ADE values are in eV and experimentally determined in this work (black, solid) or that of Davico [28] (red, dashed).

considerations lead to the energetics in Figure 5 and are discussed in more detail below.

Si_3C

Our cryo-SEVI spectrum reports solely on structure 1a of Si_3C and exhibits no evidence of the presence of another isomer, in agreement with previous anion PES studies [27]. As our ions are cooled in a clustering channel in the laser ablation source and further in a cryogenic ion trap, the ions produced by the cryo-SEVI apparatus are likely the most stable anion isomers. This suggests that 1a is the global minimum on the Si_3C^- surface, in agreement with theory [41,45]. Further, as it has been established that structure 1a is the global minimum structure of Si_3C [23], the measured ADE of Si_3C^- is the adiabatic electron affinity of Si_3C, as show in Figure 5.

Si_2C_2

It is well established that structure 2b is the global minimum for neutral Si_2C_2 whereas either 2c or 2d has been attributed to the global minimum on the anionic surface [30,33,36,39,45]. Our cryo-SEVI spectra, in combination with FC simulations, provide clear evidence that structure 2d is the anionic ground state and represent the first experimental confirmation of structure 2d for neutral Si_2C_2, the only low-lying isomer of Si_2C_2 with a dipole moment – suggesting this species may be observable in the ISM via its rotational spectrum. Bands from other isomers of Si_2C_2 in our cryo-SEVI spectra arise from higher-lying anionic states.

In accordance with these findings, our calculations suggest that structure 2d is the most stable form of $Si_2C_2^-$, with 2c and 2b residing 0.06 and 0.38 eV higher, while in the neutral species, 2d resides ∼0.2 eV above 2b and 0.13 eV below 2c (see Table 19 in SI). These calculations also predict ADEs of 1.15, 1.73, and 1.80 eV for structures 2b, 2d, and 2c of $Si_2C_2^-$, respectively, further supporting the assignments of the features observed at ∼1.30 eV, 1.9019(4), and 2.1291(8) eV as detachment from structures 2b, 2d, and 2c, respectively. The assignment of 2b is bolstered by the low relative intensity of the feature – the intensities of these two bands report on the relative populations of the two isomers, suggesting a small population of $Si_2C_2^-$ in structure 2b, as would be expected for a high-lying anion isomer in our experiment. Similarly, the integrated intensity of all features reporting on structure 2c is dramatically lower than the intensity of those reporting on structure 2d, suggesting a lower population of structure 2c than 2d.

If structures 2b, 2c, and 2d of $Si_2C_2^-$ are assumed to be degenerate, then from the measured ADE values, the neutral structure 2b resides 0.87 and 0.59 eV below structures 2c and 2d, respectively. This value, however, is an upper bound to the neutral splitting, as the 2b anion is undisputedly higher in energy than the 2c and 2d anions, with our calculations suggesting it lies 0.38 eV above the 2d ground state. A similar analysis yields an upper bound for structure 2c residing 0.299 eV above 2d, which is likely close to the actual value as the appearance of both structures 2c and 2d with similar intensity here and in the previous work by Kaya [27] suggests that the isomers have similar energetics, in agreement with our calculated energy splitting of 0.059 eV between these two anions.

SiC_3

Finally, we return to the longstanding question surrounding the ground state of SiC_3, for which theoretical reports have shown strong method-dependence on the determined ground state structure [29,36,39,40,42,43,45,46]. Previous PES studies by Kaya [27] and Lineberger [28] have confirmed the ADE of the linear structure 3f as 2.827 eV and observed two other bands with ADEs of 1.93(10) and 2.629 eV, both attributed to ring structures. Our current investigation has revisited the lowest eBE feature and shows it to originate from structure 3e, while the 2.629 eV feature from Lineberger *et al.* is found to match well with our FC-simulations for structure 3 g (Figure S12 in SI).

Much like in the case of Si_2C_2, the photodetachment transitions measured previously and here do not map onto a common neutral state. The measured ADE of structure 3e of SiC_3^- is 0.725 and 0.922 eV lower than structures 3 g and 3f, respectively, and a similar treatment to that described for Si_2C_2 gives these values as upper bounds for the energetic splitting between the neutral isomers. This is likely close to the true splitting of structures 3e and 3 g, though the latter of these upper bounds is a significant overestimation, as structures 3e and 3 g of SiC_3^- has been calculated to reside ∼0.5 eV above the linear structure 3f both here and previously [36,37,45]. These calculations are supported by previous PES studies that observe an increase in intensity of the features corresponding to the ring isomers as experimental conditions are varied to favour hotter ion production.

For structure 3e to not be the ground state of SiC_3 would require its anion to reside nearly twice as high as predicted – close to a full eV above structure 3f. As it has been established that the cryo-SEVI apparatus tends to favour production of low-lying isomers [96], the appearance of such an energetically unfavourable anion would be rather surprising. Further, we find poor signal to noise despite good ion signal, indicating a low population of structure 3e consistent with the calculated splitting of 0.5 eV. It seems unlikely, then, that the calculated energetics are in error by the factor of two required to impact the neutral ordering. Collectively, the results presented here demonstrate that structure 3e is not the ground state of SiC_3^- but favour it as the global minimum of SiC_3.

Conclusion

High resolution cryo-SEVI spectra of Si_3C^-, $Si_2C_2^-$, and SiC_3^- are presented along with high-level *ab initio* calculations. Spectral assignments are readily obtained by comparison to simulated Franck-Condon profiles, revealing forbidden transitions in each cluster, ascribed to vibronic coupling in Si_3C and SiC_3 or vibrational autodetachment in Si_2C_2. Detachment from $Si_2C_2^-$ reveals the presence of three isomers of this anion present after cryogenic cooling, allowing for the determination of structure 2d as the ground state of $Si_2C_2^-$. Reinvestigation of the low eBE region of SiC_3^- shows structure 3e is responsible for this band, providing the first vibrational characterisation of this isomer of SiC_3. Experimental ADEs are extracted from these spectra for structures 1a, 2b,c, d, and 3e of Si_3C^-, $Si_2C_2^-$, and SiC_3^-, representing an improvement of two orders of magnitude over previously reported values. Upper bounds on the energetic splitting of the Si_2C_2 and SiC_3 neutral clusters are established and suggest that the long-contested ground state of SiC_3 is a ring structure with a transannular C–C bond.

Acknowledgments

M.C.B. thanks the Army Research Office for a National Defense Science and Engineering Graduate fellowship. M.C.B. acknowledges NIH Grant No S10OD023532 for funding the computational facilities used in this work. We would like to thank Luke Bertels for productive conversations regarding Si_2C_2.

Disclosure statement

No potential conflict of interest was reported by the author(s).

Funding

This research is funded by the Air Force Office of Scientific Research under grant number FA9550-19-1-0051.

ORCID

Mark C. Babin http://orcid.org/0000-0001-7440-8058
Martin DeWitt http://orcid.org/0000-0002-1559-2112
Marissa L. Weichman http://orcid.org/0000-0002-2551-9146
Jessalyn A. DeVine http://orcid.org/0000-0003-0091-4286
Daniel M. Neumark http://orcid.org/0000-0002-3762-9473

References

[1] P. Melinon, B. Masenelli, F. Tournus and A. Perez, Nat. Mater. **6**, 479–490 (2007).
[2] Zetterling, C.-M., editor, *Process Technology for Silicon Carbide Devices* (The Institution of Electrical Engineers, New York, 2002).
[3] P. Thaddeus, S.E. Cummins and R.A. Linke, Astrophys. J. **283**, L45–L48 (1984).
[4] J. Cernicharo, C.A. Gottlieb, M. Guelin, P. Thaddeus and J.M. Vrtilek, Astrophys. J. **341**, L25–L28 (1989).
[5] M. Ohishi, N. Kaifu, K. Kawaguchi, A. Murakami, S. Saito, S. Yamamoto, S. Ishikawa, Y. Fujita, Y. Shiratori and W.M. Irvine, Astrophys. J. **345**, L83–L86 (1989).
[6] A.J. Apponi, M.C. McCarthy, C.A. Gottlieb and P. Thaddeus, Astrophys. J. **516**, L103–L106 (1999).
[7] A.J. Apponi, M.C. McCarthy, C.A. Gottlieb and P. Thaddeus, J. Chem. Phys. **111**, 3911–3918 (1999).
[8] J. Cernicharo, M.C. McCarthy, C.A. Gottlieb, M. Agundez, L.V. Prieto, J.H. Baraban, P.B. Changala, M. Guelin, C. Kahane, M.A. Martin-Drumel, N.A. Patel, N.J. Reilly, J.F. Stanton, G. Quintana-Lacaci, S. Thorwirth, and K.H. Young, Astrophys. J. Lett. **806**, L3 (2015).
[9] K.S. Pitzer and E. Clementi, J. Am. Chem. Soc. **81**, 4477–4485 (1959).
[10] K. Raghavachari and J.S. Binkley, J. Chem. Phys. **87**, 2191–2197 (1987).
[11] R.E. Smalley, Accounts Chem. Res. **25**, 98–105 (1992).
[12] E.C. Honea, A. Ogura, C.A. Murray, K. Raghavachari, W.O. Sprenger, M.F. Jarrold and W.L. Brown, Nature **366**, 42–44 (1993).
[13] G. Von Helden, M.T. Hsu, N. Gotts and M.T. Bowers, J. Phys. Chem.-Us **97**, 8182–8192 (1993).
[14] J.M.L. Martin, J. Elyazal and J.P. Francois, Chem. Phys. Lett. **242**, 570–579 (1995).
[15] S. Li, R.J. Van Zee, W. Weltner and K. Raghavachari, Chem. Phys. Lett. **243**, 275–280 (1995).
[16] J.M.L. Martin and P.R. Taylor, J. Phys. Chem.-Us **100**, 6047–6056 (1996).
[17] C.S. Xu, T.R. Taylor, G.R. Burton and D.M. Neumark, J. Chem. Phys. **108**, 1395–1406 (1998).
[18] J.D. Presillamarquez and W.R.M. Graham, J. Chem. Phys. **96**, 6509–6514 (1992).
[19] J.D. Presillamarquez, S.C. Gay, C.M.L. Rittby and W.R.M. Graham, J. Chem. Phys. **102**, 6354–6361 (1995).
[20] M.C. McCarthy, A.J. Apponi and P. Thaddeus, J. Chem. Phys. **111**, 7175–7178 (1999).
[21] M.C. McCarthy, A.J. Apponi and P. Thaddeus, J. Chem. Phys. **110**, 10645–10648 (1999).
[22] M.C. McCarthy, A.J. Apponi, C.A. Gottlieb and P. Thaddeus, Astrophys. J. **538**, 766–772 (2000).
[23] J.F. Stanton, J. Dudek, P. Theule, H. Gupta, M.C. McCarthy, and P. Thaddeus, J. Chem. Phys. **122**, 124314 (2005).
[24] N.J. Reilly, M. Steglich, D.L. Kokkin, J.P. Maier, J.F. Stanton and M.C. McCarthy, J. Mol. Spectrosc. **310**, 135–140 (2015).
[25] M. Steglich and J.P. Maier, Astrophys. J. **801**, 119 (2015).
[26] N.X. Truong, M. Savoca, D.J. Harding, A. Fielicke and O. Dopfer, Phys. Chem. Chem. Phys. **17**, 18961–18970 (2015).
[27] A. Nakajima, T. Taguwa, K. Nakao, M. Gomei, R. Kishi, S. Iwata and K. Kaya, J. Chem. Phys. **103**, 2050–2057 (1995).
[28] G.E. Davico, R.L. Schwartz and W.C. Lineberger, J. Chem. Phys. **115**, 1789–1794 (2001).

[29] J.F. Stanton, J. Gauss and O. Christiansen, J. Chem. Phys. **114**, 2993–2995 (2001).

[30] G.W. Trucks and R.J. Bartlett, J. Mol. Struc.-Theochem. **28**, 423–428 (1986).

[31] K. Lammertsma and O.F. Guner, J. Am. Chem. Soc. **110**, 5239–5245 (1988).

[32] P.V. Sudhakar, O.F. Guner and K. Lammertsma, J. Phys. Chem.-Us **93**, 7289–7292 (1989).

[33] G.B. Fitzgerald and R.J. Bartlett, Int. J. Quantum Chem. **38**, 121–128 (1990).

[34] I.L. Alberts, R.S. Grev and H.F. Schaefer, J. Chem. Phys. **93**, 5046–5052 (1990).

[35] C.M.L. Rittby, J. Chem. Phys. **96**, 6768–6772 (1992).

[36] S. Hunsicker and R.O. Jones, J. Chem. Phys. **105**, 5048–5060 (1996).

[37] M. Gomei, R. Kishi, A. Nakajima, S. Iwata and K. Kaya, J. Chem. Phys. **107**, 10051–10061 (1997).

[38] P. Bandyopadhyay, S. Ten-no and S. Iwata, J. Phys. Chem. A **103**, 6442–6447 (1999).

[39] J.M. Rintelman and M.S. Gordon, J. Chem. Phys. **115**, 1795–1803 (2001).

[40] K.W. Sattelmeyer, H.F. Schaefer and J.F. Stanton, J. Chem. Phys. **116**, 9151–9153 (2002).

[41] Z.Y. Jiang, X.H. Xu, H.S. Wu and Z.H. Jin, J. Phys. Chem. A **107**, 10126–10131 (2003).

[42] Y. Kurashige, H. Nakano and K. Hirao, J. Phys. Chem. A **108**, 3064–3067 (2004).

[43] J.M. Rintelman, M.S. Gordon, G.D. Fletcher, and J. Ivanic, J. Chem. Phys. **124**, 034303 (2006).

[44] R. Linguerri, P. Rosmus, and S. Carter, J. Chem. Phys. **125**, 034305 (2006).

[45] X.F. Duan, J. Wei, L. Burggraf and D. Weeks, Comp. Mater. Sci. **47**, 630–644 (2010).

[46] T. Yang, L. Bertels, B.B. Dangi, X.H. Li, M. Head-Gordon and R.I. Kaiser, P. Natl. Acad. Sci. U.S.A. **116**, 14471–14478 (2019).

[47] C. Hock, J.B. Kim, M.L. Weichman, T.I. Yacovitch, and D.M. Neumark, J. Chem. Phys. **137**, 244201 (2012).

[48] A. Osterwalder, M.J. Nee, J. Zhou and D.M. Neumark, J. Chem. Phys. **121**, 6317–6322 (2004).

[49] D.M. Neumark, J. Phys. Chem. A **112**, 13287–13301 (2008).

[50] M.L. Weichman and D.M. Neumark, Annu. Rev. Phys. Chem. **69**, 101–124 (2018).

[51] U. Even, J. Jortner, D. Noy, N. Lavie and C. Cossart-Magos, J. Chem. Phys. **112**, 8068–8071 (2000).

[52] J.B. Kim, C. Hock, T.I. Yacovitch and D.M. Neumark, J. Phys. Chem. A **117**, 8126–8131 (2013).

[53] J.A. DeVine, M.L. Weichman, B. Laws, J. Chang, M.C. Babin, G. Balerdi, C.J. Xie, C.L. Malbon, W.C. Lineberger, D.R. Yarkony, R.W. Field, S.T. Gibson, J.Y. Ma, H. Guo and D.M. Neumark, Science **358**, 336–339 (2017).

[54] W.C. Wiley and I.H. Mclaren, Rev. Sci. Instrum. **26**, 1150–1157 (1955).

[55] A.T.J.B. Eppink and D.H. Parker, Rev. Sci. Instrum. **68**, 3477–3484 (1997).

[56] M.L. Weichman, J.A. DeVine, D.S. Levine, J.B. Kim and D.M. Neumark, P. Natl. Acad. Sci. U.S.A. **113**, 1698–1705 (2016).

[57] D.W. Chandler and P.L. Houston, J. Chem. Phys. **87**, 1445–1447 (1987).

[58] M.B. Doyle, C. Abeyasera, A.G. Suits (2017).

[59] B. Dick, Phys. Chem. Chem. Phys. **16**, 570–580 (2014).

[60] C. Blondel, W. Chaibi, C. Delsart, C. Drag, F. Goldfarb and S. Kroger, Eur. Phys. J. D **33**, 335–342 (2005).

[61] J. Cooper and R.N. Zare, J. Chem. Phys. **48**, 942–943 (1968).

[62] A. Sanov, Annu. Rev. Phys. Chem. **65**, 341–363 (2014).

[63] R.A. Kendall, T.H. Dunning and R.J. Harrison, J. Chem. Phys. **96**, 6796–6806 (1992).

[64] J.D. Watts, J. Gauss and R.J. Bartlett, J. Chem. Phys. **98**, 8718–8733 (1993).

[65] P.J. Knowles, C. Hampel and H.J. Werner, J. Chem. Phys. **99**, 5219–5227 (1993).

[66] M.J. Frisch, G.W. Trucks, H.B. Schlegel, G.E. Scuseria, M.A. Robb, J.R. Cheeseman, G. Scalmani, V. Barone, G.A. Petersson, H. Nakatsuji, X. Li, M. Caricato, A.V. Marenich, J. Bloino, B.G. Janesko, R. Gomperts, B. Mennucci, H.P. Hratchian, J.V. Ortiz, A.F. Izmaylov, J.L. Sonnenberg, D. Williams-Young, F. Ding, F. Lipparini, F. Egidi, J. Goings, B. Peng, A. Petrone, T. Henderson, D. Ranasinghe, V.G. Zakrzewski, J. Gao, N. Rega, G. Zheng, W. Liang, M. Hada, M. Ehara, K. Toyota, R. Fukuda, J. Hasegawa, M. Ishida, T. Nakajima, Y. Honda, O. Kitao, H. Nakai, T. Vreven, K. Throssell, J.A. Montgomery, J.E. Peralta, F. Ogliaro, M.J. Bearpark, J.J. Heyd, E.N. Brothers, K.N. Kudin, V.N. Staroverov, T.A. Keith, R. Kobayashi, J. Normand, K. Raghavachari, A.P. Rendell, J.C. Burant, S.S. Iyengar, J. Tomasi, M. Cossi, J.M. Millam, M. Klene, C. Adamo, R. Cammi, J.W. Ochterski, R.L. Martin, K. Morokuma, O. Farkas, J.B. Foresman and D.J. Fox (Gaussian, Inc, Wallingford, CT, 2016).

[67] V.A. Mozhayskiy and Anna I. Krylov, *ezSpectrum v3.0* (iOpenShell Center for Computational Studies of Electronic Structure and Spectroscopy of Open-Shell and Electronically Excited Species, Los, Angeles) < http://iopenshell.usc.edu/downloads > .

[68] F. Duschinsky, Acta Physicochim. Urs. **7**, 551–566 (1937).

[69] H.J. Monkhorst, Int. J. Quantum Chem. **12**, 421–432 (1977).

[70] K. Emrich, Nucl. Phys. A **351**, 397–438 (1981).

[71] E. Dalgaard and H.J. Monkhorst, Phys. Rev. A **28**, 1217–1222 (1983).

[72] S. Ghosh and D. Mukherjee, P. Ind.-Chem. Sci. **93**, 947–963 (1984).

[73] J. Geertsen, M. Rittby and R.J. Bartlett, Chem. Phys. Lett. **164**, 57–62 (1989).

[74] H. Koch and P. Jorgensen, J. Chem. Phys. **93**, 3333–3344 (1990).

[75] K.M. Ervin and W.C. Lineberger, J. Phys. Chem.-Us **95**, 1167–1177 (1991).

[76] C.G. Bailey, C.E.H. Dessent, M.A. Johnson and K.H. Bowen, J. Chem. Phys. **104**, 6976–6983 (1996).

[77] K.R. Asmis, T.R. Taylor and D.M. Neumark, J. Chem. Phys. **111**, 8838–8851 (1999).

[78] J. Zhou, E. Garand, and D.M. Neumark, J. Chem. Phys. **127**, 154320 (2007).

[79] T. Ichino, S.W. Wren, K.M. Vogelhuber, A.J. Gianola, W.C. Lineberger, and J.F. Stanton, J. Chem. Phys. **129**, 084310 (2008).

[80] D.L. Huang, P.D. Dau, H.T. Liu, and L.S. Wang, J. Chem. Phys. **140**, 224315 (2014).

[81] M.L. Weichman, L. Cheng, J.B. Kim, J.F. Stanton, and D.M. Neumark, J. Chem. Phys. **146**, 224309 (2017).

[82] S.J. Kregel, G.K. Thurston, and E. Garand, J. Chem. Phys. **148**, 234306 (2018).
[83] J.A. DeVine, A. Abou Taka, M.C. Babin, M.L. Weichman, H.P. Hratchian, and D.M. Neumark, J. Chem. Phys. **148**, 222810 (2018).
[84] M.C. Babin, J.A. DeVine, M. DeWitt, J.F. Stanton and D.M. Neumark, J. Phys. Chem. Lett. **11**, 395–400 (2020).
[85] H.T. Liu, C.G. Ning, D.L. Huang, P.D. Dau and L.S. Wang, Angew. Chem. Int. Edit. **52**, 8976–8979 (2013).
[86] M.L. Weichman, J.B. Kim, and D.M. Neumark, J. Chem. Phys. **140**, 104305 (2014).
[87] D.L. Huang, H.T. Liu, C.G. Ning, and L.S. Wang, J. Chem. Phys. **142**, 124309 (2015).
[88] D.L. Huang, H.T. Liu, C.G. Ning, G.Z. Zhu and L.S. Wang, Chem. Sci. **6**, 3129–3138 (2015).
[89] J.A. DeVine, M.L. Weichman, C.J. Xie, M.C. Babin, M.A. Johnson, J.Y. Ma, H. Guo and D.M. Neumark, J. Phys. Chem. Lett. **9**, 1058–1063 (2018).
[90] J. Simons, J. Am. Chem. Soc. **103**, 3971–3976 (1981).
[91] T. Andersen, K.R. Lykke, D.M. Neumark and W.C. Lineberger, J. Chem. Phys. **86**, 1858–1867 (1987).
[92] D.W. Arnold, S.E. Bradforth, T.N. Kitsopoulos and D.M. Neumark, J. Chem. Phys. **95**, 8753–8764 (1991).
[93] C.S. Xu, G.R. Burton, T.R. Taylor and D.M. Neumark, J. Chem. Phys. **107**, 3428–3436 (1997).
[94] M.L. Weichman, J.B. Kim, and D.M. Neumark, J. Chem. Phys. **139**, 144314 (2013).
[95] M.C. Babin, J.A. DeVine, M.L. Weichman and D.M. Neumark, J. Chem. Phys. **149**, 174306 (2018).
[96] J.B. Kim, M.L. Weichman and D.M. Neumark, J. Am. Chem. Soc. **136**, 7159–7168 (2014).